

# Disorder-mediated synchronization resonance in coupled semiconductor lasers

Li-Li Ye,<sup>1</sup> Nathan Vigne,<sup>2</sup> Fan-Yi Lin,<sup>2,3</sup> Hui Cao,<sup>2,\*</sup> and Ying-Cheng Lai<sup>1,4,†</sup>

<sup>1</sup>*School of Electrical, Computer and Energy Engineering,  
Arizona State University, Tempe, Arizona 85287, USA*

<sup>2</sup>*Department of Applied Physics, Yale University, New Haven, Connecticut 06520, USA*

<sup>3</sup>*Institute of Photonics Technologies, Department of Electrical Engineering,  
National Tsing Hua University, Hsinchu 30013, Taiwan*

<sup>4</sup>*Department of Physics, Arizona State University, Tempe, Arizona 85287, USA*

(Dated: September 10, 2025)

The interplay between disorder and synchronization in nonlinear oscillator networks has long been known to give rise to counterintuitive phenomena, such as disorder-enhanced coherence. We uncover a frequency-disorder mediated synchronization resonance in coupled external-cavity semiconductor diode lasers. Specifically, we find that intrinsic random frequency detuning among the lasers can enhance synchronization, reaching a maximum at an optimal coupling strength in the weak-coupling regime. The resonance is genuinely disorder-mediated, as it vanishes in the corresponding disorder-free system. To explain this phenomenon, we develop a physical theory based on an effective thermodynamic potential, which also accounts for the associated scaling behavior. Our results establish semiconductor laser arrays as a versatile experimental platform for investigating disorder-driven collective dynamics, with potential implications for a broad class of nonlinear systems.

Synchronization in complex dynamical systems has been a topic of continuous interest [1, 2]. A common setting is coupled dynamical oscillators, where the bifurcation parameter is the coupling strength among the oscillators. A focus of many previous studies was on identifying the critical point at which a transition from desynchronization to synchronization occurs. Depending on the dynamics of the oscillators and the coupling function, the system can have a sequence of transitions, giving rise to characteristically distinct synchronization behaviors in the parameter space. For example, for a system of coupled identical nonlinear oscillators, complete synchronization can arise when the coupling exceeds a critical strength as determined by the master stability function [3, 4]. Systems of phase oscillators with nonlinear coupling, e.g., those described by the classic Kuramoto model [1], can host phase synchronization and the critical coupling strength required for the onset of this type of “weak” synchronization can be determined by the mean-field theory [5, 6]. Synchronization in coupled oscillators was experimentally studied [7, 8]. A counterintuitive phenomenon is that adding connections can hinder network synchronization of time-delayed oscillators [9]. Biomedical applications of synchronization have also been actively studied [10].

There is large literature on synchronization in networks of nonlinear oscillators [11]. A remarkable phenomenon is that disorders, e.g., random parameter heterogeneity among the oscillators, can counter-intuitively maximize [12] and promote [13, 14] synchronization. For coupled chaotic oscillators, parameter regimes can arise where the oscillator heterogeneity leads to synchronization for conditions under which identical oscillators can-

not be synchronized [15]. Synchronization in networked systems with large parameter mismatches was studied in terms of the stability of the synchronous state and transition [16]. Of physical significance with considerable theoretical and experimental interests are external-cavity semiconductor lasers [17–28], mathematically described by the time-delayed nonlinear Lang–Kobayashi (LK) equations [29]. For an array of fully coupled semiconductor lasers, a recent theoretical work advocated the idea of achieving and enhancing synchronization by exploiting disorders [19], where synchronization was demonstrated through time-delay induced disorders to compensate for the intrinsic frequency mismatch.

In this Letter, we report a disorder-mediated synchronization resonance in semiconductor diode laser arrays with homogeneous, all-to-all coupling. While such a network of identical lasers can readily synchronize, realistic systems exhibit random and heterogeneous frequency detuning, e.g., as generated in the manufacturing process, which can suppress synchronization in the weakly coupled regime [19]. We find that increasing the coupling from zero produces a resonance at which synchronization is maximized for an optimal coupling strength, at which the lasers exhibit strong collective coherence in the form of frequency and phase locking. To explain this resonance phenomenon, we develop a theory that recasts the delayed phase dynamics as a gradient flow on an effective thermodynamic potential, where the steady-state solutions correspond to local minima of the potential. This framework quantitatively establishes the resonance and its scaling law, revealing a key physical mechanism for such a resonance to emerge: the coupling between amplitude and phase dynamics. While it has been qualitatively known by the laser community that coupling cannot be arbitrarily weak or excessively strong for synchronization, the uncovered resonance phenomenon in semiconductor lasers has not been previously reported.

\* hui.cao@yale.edu

† Ying-Cheng.Lai@asu.edu

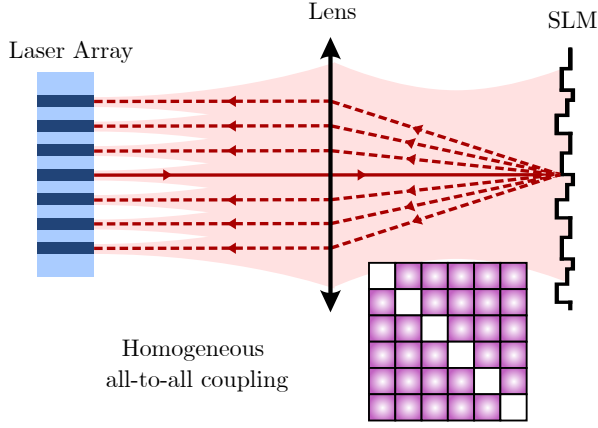


FIG. 1. Illustration of a network of coupled semiconductor diode lasers. Experimentally, the coupling configuration can be realized by a spatial light modulator placed in the back focal plane of a collimation lens.

A network of  $M$  coupled diode lasers, each operating in a single longitudinal and transverse mode at fixed polarization with frequency disorders, is described by the LK equations [19, 29]:

$$\begin{aligned} \frac{dE_i(t)}{dt} &= \frac{1+i\alpha}{2} \left( g \frac{N_i(t) - N_0}{1+s|E_i(t)|^2} - \gamma \right) E_i(t) \\ &\quad + i\Delta_i E_i(t) + e^{-i\omega_0\tau} \sum_{j=1}^M K_{ij} E_j(t-\tau), \\ \frac{dN_i(t)}{dt} &= J_0 - \gamma_n N_i(t) - g \frac{N_i(t) - N_0}{1+s|E_i(t)|^2} |E_i(t)|^2, \end{aligned} \quad (1)$$

where  $E_i(t)$  is the complex electric field of the  $i$ th laser,  $N_i(t)$  is the carrier number governed by the pump rate  $J_0 = 4J_{th}$  with  $J_{th} = \gamma_n(N_0 + \gamma/g)$  being the single-laser pump rate at threshold,  $\gamma_n$  is the carrier loss rate,  $N_0$  is the carrier number at transparency,  $\gamma$  is the cavity loss rate,  $g$  is the differential gain coefficient, and  $\tau$  is the time delay due to the external cavity. The typical experimental parameter values are  $\gamma_n = 0.5 \text{ ns}^{-1}$ ,  $N_0 = 1.5 \times 10^8$ ,  $\gamma = 500 \text{ ns}^{-1}$ , and  $g = 1.5 \times 10^{-5} \text{ ns}^{-1}$ . Other experimental parameter values are: the amplitude-phase coupling (linewidth enhancement) factor  $\alpha = 5$ , gain saturation coefficient  $s = 2 \times 10^{-7}$ , and external time delay  $\tau = 3 \text{ ns}$ . Random frequency disorders are modeled as  $\Delta_i = \sigma_\Delta \mathcal{N}(0, 1)$ , where  $\mathcal{N}(0, 1)$  is a Gaussian random variable with zero mean and unit variance. The natural angular frequency reference  $\omega_0$  is chosen such that  $\omega_0\tau = 2N\pi$  with  $N$  selected to be closest to the mean of all natural angular frequencies. The frequency disorder values are ordered as  $\Delta_1 \leq \Delta_2 \leq \dots \leq \Delta_M$ , with  $\sigma_\Delta = 14 \text{ rad/ns}$  and  $M = 24$ .

The laser field is  $E_i(t) = r_i(t)e^{i\Omega_i(t)}$ . Synchronization encompassing amplitude, frequency and phase can be quantified by  $\langle S \rangle = \langle |\sum_{i=1}^M E_i(t)|^2 / [M \sum_{i=1}^M |E_i(t)|^2] \rangle \in [0, 1]$ , where a higher value corresponds to stronger synchronization. The all-to-all coupling configuration is

described by  $K_{ij} = \kappa(1 - \delta_{ij})$ , with  $\kappa$  and  $\delta_{ij}$  being the coupling strength and Kronecker delta, respectively. Without frequency disorders, complete synchronization ( $\langle S \rangle = 1$ ) occurs even in the weakly coupling regime.

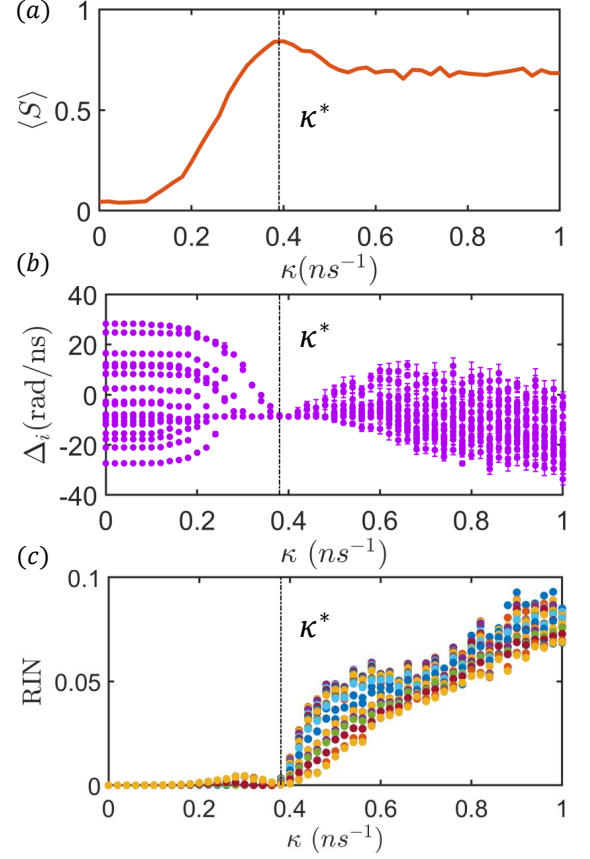


FIG. 2. Disorder-mediated synchronization resonance in a network of  $M = 24$  semiconductor diode lasers. (a) Maximization of synchronization measures  $\langle S \rangle$  by an optimal coupling strength  $\kappa^*$ . (b) Average short-term final frequency detuning of the individual lasers versus  $\kappa$ , where the error bars represent the standard deviation calculated over a moving time window of size  $3\tau$  with a step size of  $0.3\tau$  for  $t \in [50, 100] \text{ ns}$ . (c) MS (mean-square) value of the relative intensity noise for the individual lasers over a 50 ns time window, defined as the variance of normalized intensity fluctuations  $\sqrt{\langle (I(t) - \langle I \rangle)^2 \rangle / \langle I \rangle}$ , versus  $\kappa$ .

When frequency disorders are present, a resonance emerges in the weakly coupling regime  $\kappa \in [0, 1] \text{ ns}^{-1}$ :  $\langle S \rangle$  is maximized by a proper amount of coupling. For example, for  $M = 24$  lasers, we have  $\langle S \rangle_{\max} \approx 0.84$  for  $\kappa^* \approx 0.4 \text{ ns}^{-1}$ , as shown in Fig. 2(a). Figures 2(b) and 2(c) display the fitted short-term frequencies and the fluctuations of the normalized intensities for  $M = 24$ , respectively. Our computations revealed that, in the presence of frequency disorders, the strong synchronization achieved through the resonance is in fact steady-state synchronization, where the individual lasers maintain sinusoidal, nearly synchronous oscillations. This type of synchronization is desired in applications. While chaotic

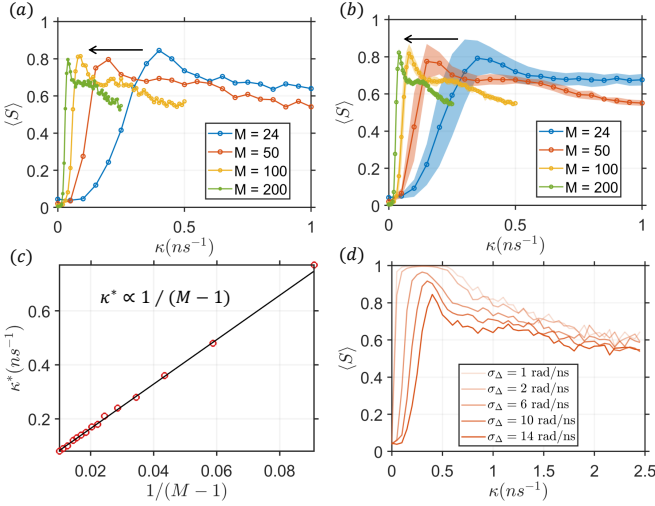


FIG. 3. Robustness and size scaling of synchronization resonance. The frequency disorders are independently sampled from a Gaussian distribution  $\sigma_\Delta \mathcal{N}(0, 1)$  with the standard deviation  $\sigma_\Delta$ . (a) Synchronization resonance for different number  $M$  of lasers for  $\sigma_\Delta = 14 \text{ rad/ns}$ . (b) Statistical fluctuations of the resonance, where for each value of  $M$ , ten independent realizations of the frequency disorder for  $\sigma_\Delta = 14 \text{ rad/ns}$  are tested. The four curves in their respective statistical clouds are the averages and the shaded areas indicate the corresponding standard deviations. (c) Location of the resonance peak,  $\kappa^*$ , indicated by the averaged peak position over ten frequency disorder realizations. The resulting  $\kappa^*$  values exhibit an inverse relationship with the system size:  $\kappa^* \propto 1/(M-1)$ , demonstrated for  $M = [12, 18, 24, 30, 36, 42, 46, 50, 55, 60, 65, 70, 80, 90, 100]$ . (d) Effect of frequency disorder strength as characterized by  $\sigma_\Delta$  on the synchronization resonance for  $M = 24$ . For small values of  $\sigma_\Delta$ , the peak value of  $\langle S \rangle$  can reach unity as in the corresponding disorder-free system.

synchronization can be achieved in the strong coupling regime [19, 30, 31], it is not the focus of our study.

Heuristically, the underlying mechanism of the resonance is as follows. For  $\kappa = 0$  and with frequency disorders, synchronization is not possible. For small values of  $\kappa$ , the coupling is insufficient to counter the frequency detuning, yielding only marginal improvement in synchronization. As  $\kappa$  increases, insofar as the laser dynamics are regular (not chaotic), synchronization is continuously enhanced. This increasing trend stops when irregular dynamics sets in, as revealed by Figs. 2(b) and 2(c), leading to a decrease in the synchronization measure  $\langle S \rangle$  as  $\kappa$  further increases. For sufficiently strong coupling  $\kappa \gg \kappa^*$ , the disruptive influence of the disorders on synchronization diminishes and chaotic synchronization emerges.

Is the phenomenon of synchronization resonance robust as the laser network becomes larger? Figure 3 provides an affirmative answer. As the network size  $M$  increases, the optimal coupling value  $\kappa^*$  decreases, but the resonance persists, as shown in Fig. 3(a). This can be understood by noting that the total coupling per laser  $\sum_j K_{ij} = \kappa(M-1)$  is assumed to be fixed as in a re-

alistic experimental setting. If approximately the same amount of total coupling per laser is required for the resonance to arise, increasing  $M$  will naturally result in a reduced  $\kappa^*$  value. As  $M$  increases, the statistical variation of the frequency disorder becomes well behaved, leading to narrower fluctuations in the synchronization resonance, as shown in Fig. 3(b). The height of the resonance peak in  $\langle S \rangle$  with increasing  $M$  remains approximately constant, due to the fact that, at the resonance peak, the total coupling strength per laser remains constant, thereby preserving the steady-state solution and sustaining the same level of synchronization, as explained by our theory below. Quantitatively, the dependence of  $\kappa^*$  on  $M$  follows the scaling relation:  $\kappa^* \propto 1/(M-1)$ , as shown in Fig. 3(c). For  $M = 2$  ( $M = 24$ ) coupled lasers, the optimal coupling is  $\kappa^* \approx 8 \text{ ns}^{-1}$  ( $\kappa^* \approx 0.4 \text{ ns}^{-1}$ ) [Fig. 3(c)]. This demonstrates that *more is different*: increasing the number of lasers markedly reduces the required coupling per link ( $\kappa^*$ ), while the optimal total coupling cost,  $\sum_{ij} K_{ij}^* \propto M$ , scales linearly with  $M$  (supported by our physical theory below). In addition, as the extent of frequency disorder measured by the standard deviation  $\sigma_\Delta$  of the frequency distribution is reduced, synchronization is enhanced, as shown in Fig. 3(d).

To explain the synchronization resonance in Figs. 3(a–d), we develop a physical theory by expanding the LK equations about the steady state, yielding a generalized time-delayed Kuramoto system [32] with an additional phase shift  $\tan^{-1} \alpha + \omega_0 \tau$  and an effective coupling enhanced by the amplitude-phase coupling  $\sqrt{1 + \alpha^2}$  [Sec. III in Supplementary Information (SI)]. Introducing the delayed phase differences  $\eta_i = \Omega_i(t) - \Omega_i(t - \tau)$ , the dynamics can be recast as a gradient flow governed by an effective thermodynamic potential  $U(\eta_i)$ , which encapsulates the collective coupling influence of the other lasers on laser  $i$ . In the absence of frequency disorder ( $\Delta_i = \Delta_j = 0$ ) with all lasers oscillating at the reference frequency  $\omega_0$ , the coupling configuration  $K_{ij} = \kappa(1 - \delta_{ij})$  renders the identical potential across the lasers:

$$U(\eta(t)) = \eta^2(t) - 2\tau\sqrt{1 + \alpha^2}k^{\text{in}} \cos[\eta(t) + \tan^{-1} \alpha + \omega_0 \tau], \quad (2)$$

where  $k^{\text{in}} = \sum_j K_{ij} = \kappa(M-1)$  is the intrinsic coupling strength received by each laser from the others. The local minima of  $U(\eta)$  coincide for all lasers at  $\eta^* = 2\pi f_{\text{final}}\tau$  that defines the synchronized frequency. The first quadratic term enforces parabolic confinement, while the cosine modulation arises from delay  $\tau$ , amplitude-phase coupling parameter  $\alpha$ , and intrinsic coupling  $k^{\text{in}}$ . For weak effective coupling  $\mathbb{K} \equiv \tau\sqrt{1 + \alpha^2}\kappa(M-1) \ll \eta^2$ , the modulation is negligible and the system is in a unique synchronized steady state. In contrast, strong coupling ( $\mathbb{K} \sim \eta^2$ ) generates multiple local minima leading to multistability that drives the system into chaotic synchronization for  $\alpha \neq 0$  (see SI).

In the system governed by a smooth quadratic (parabolic) potential without coupling, as indicated by

Eq. (2), once the coupling-induced cosine oscillation is excluded, frequency disorder ( $\Delta_i \neq \Delta_j$ ) contributes an additional term  $-2\tau\Delta_i\eta_i(t)$  to the thermodynamic potential  $U(\eta_i(t))$ . As a result, the global minima of the individual lasers become substantially different, hindering synchronization. However, for sufficiently strong coupling, the potential landscape is reshaped by the cosine term in Eq. (2), producing multiple local minima separated by high barriers while leaving the distant global minima unchanged, as shown in Fig. 4(a) for two distinct initial values of detuning  $\Delta_i$ . For a fixed effective coupling  $\mathbb{K}$ , the height of the barriers separating the local minima decreases monotonically with increasing  $\eta$  from the global minimum. In the near-overlapping regime, e.g., the red rectangle in Fig. 4(a), the proximity of these local minima leads to nearly synchronized final frequencies. This mechanism enables enhanced frequency and phase locking, even though the system ultimately settles into states that are not global minima.

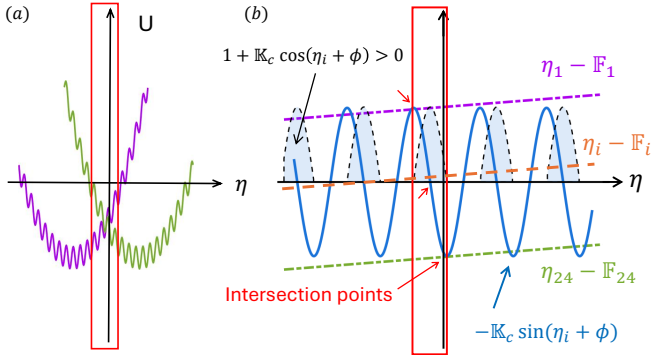


FIG. 4. Schematic of local-minima selection, corresponding to the steady state of each laser. (a) Effective thermodynamic potential comprising a parabolic term, a shifted global minimum  $-2\tau\Delta_i\eta_i(t)$ , and a coupling-induced cosine component. The red rectangle marks the near-overlapping regime that yields nearly synchronized final frequencies. (b) Illustration of steady-state selection from the local minima of the effective potential landscape for different lasers at the critical effective coupling  $\mathbb{K}_c$ .

More specifically, the local minima of the potential are determined by the conditions  $dU/d\eta_i = 0$  and  $d^2U/d\eta_i^2 > 0$ , leading to the constraints  $\eta_i - \mathbb{F}_i = -\mathbb{K} \sin(\eta_i + \phi)$  and  $1 + \mathbb{K} \cos(\eta_i + \phi) > 0$ , respectively, where  $\mathbb{F}_i \equiv \tau\Delta_i$  denotes the effective detuning and  $\phi \equiv \text{mod}(\tan^{-1} \alpha + \omega_0\tau, 2\pi) \approx 0.4\pi$ . Given the critical effective coupling  $\mathbb{K}_c$ , the intersections between the straight lines  $\eta_i - \mathbb{F}_i$  and the sinusoidal curves  $-\mathbb{K}_c \sin(\eta_i + \phi)$  that satisfy  $d^2U/d\eta_i^2 > 0$  define the local minima of the potential, i.e., the steady-state solutions  $\eta_i$  for each laser  $i$ , as illustrated in Fig. 4(b). The corresponding local minima  $\eta_i$  determine the final frequencies of the lasers. For small coupling  $\mathbb{K} \ll \mathbb{K}_c$ , laser frequencies remain widely separated, whereas large coupling  $\mathbb{K} \gg \mathbb{K}_c$  induces multistability and chaos via unstable dynamical invariant sets. There exists a critical effective coupling deter-

mined by  $\mathbb{K}_c = \max(|\mathbb{F}_i|)$ , at which all lasers attain their final frequencies within the same regime satisfying  $1 + \mathbb{K} \cos(\eta_i + \phi) > 0$ , ensuring the local minimum condition  $d^2U/d\eta_i^2 > 0$ , as highlighted by the red square in Fig. 4(b). In this case, the maximum frequency difference is determined by the width of the regime where  $d^2U/d\eta_i^2 > 0$ . The onset of such solutions defines the critical effective coupling with the resulting states referred to as near-synchronized steady states. Below this threshold, only a subset of lasers achieve closely aligned final frequencies within the same  $1 + \mathbb{K} \cos(\eta_i + \phi) > 0$  regime.

Beyond this critical effective coupling, the final frequency differences diminish and multiple stable yet distinct near-synchronized steady states emerge. As their stability weakens, synchronization begins to saturate, giving rise to periodic or quasiperiodic phase dynamics. As the coupling strength increases further, the nontrivial amplitude-phase coupling in the LK equation (see SI) can trigger chaos [25, 33], thereby weakening synchronization. The onset of chaos defines the resonance peak at  $\kappa^*$ , as shown in Fig. 2, which typically occurs slightly above the critical coupling strength, as  $\kappa^* > \kappa_c$ , where  $\kappa_c$  is determined from the critical effective coupling  $\mathbb{K}_c$ . In contrast, for  $\alpha = 0$ , the resonance vanishes: synchronized steady states appear only in the strong-coupling regime ( $\kappa \gg \kappa^*$ ), while for weak coupling ( $\kappa \sim \kappa^*$ ) the system is far away from synchronization (see SI).

More specifically, for the frequency disorder  $\Delta_i = 14 \times \mathcal{N}(0, 1)$  rad/ns, the maximum effective detuning is  $\max(|\mathbb{F}_i|) = \tau|\Delta_0| \approx 90$ . To compensate for it, the effective coupling  $\mathbb{K}^*$  must exceed  $\mathbb{K}_c = \tau|\Delta_0|$ , giving  $\kappa^* > \kappa_c = |\Delta_0|/[(M-1)\sqrt{1+\alpha^2}] \approx 0.26 \text{ ns}^{-1}$  for  $M = 24$ , which is consistent with Fig. 3. This relationship reveals the scaling  $\kappa^* \propto 1/(M-1)$ , thereby explaining the numerical results in Fig. 3(c). Moreover, the critical coupling coincides with the necessary condition of the classical Kuramoto model [34–36] in the limit of vanishing amplitude-phase coupling and time delay.

To summarize, we uncover a frequency-disorder mediated synchronization resonance in coupled diode laser networks and develop a physical theory to explain its origin and scaling behavior. The phenomenon arises from the interplay of the coupling between the amplitude and phase dynamics as well as time delay, leading to a size-scaling law that persists from small to arbitrarily large networks. Remarkably, the peak value of the synchronization level is independent of the number of lasers, with the required coupling cost scaling linearly with the system size, thereby ensuring robust synchronization in large arrays. Beyond diode lasers, our results can be extended to vertical-cavity surface-emitting lasers (VCSELs) and other classes of nonlinear oscillators. The findings go beyond the Kuramoto paradigm and establish semiconductor laser networks as a fertile platform for exploring disorder-enhanced collective dynamics.

This work was supported by the Office of Naval Research under Grant No. N00014-24-1-2548.

Supplementary Information for  
**Disorder-mediated synchronization resonance in coupled semiconductor lasers**

Li-Li Ye, Nathan Vigne, Fan-Yi Lin, Hui Cao, and Ying-Cheng Lai

Corresponding authors: Ying-Cheng Lai (Ying-Cheng.Lai@asu.edu) and Hui Cao (hui.cao@yale.edu)

## CONTENTS

A. Amplitude–phase coupling and synchronization in the absence of disorder	6
B. Disorder-induced resonance and chaos driven by amplitude–phase coupling	6
C. Effective thermodynamic potential for the laser network	7
References	9

## Appendix A: Amplitude–phase coupling and synchronization in the absence of disorder

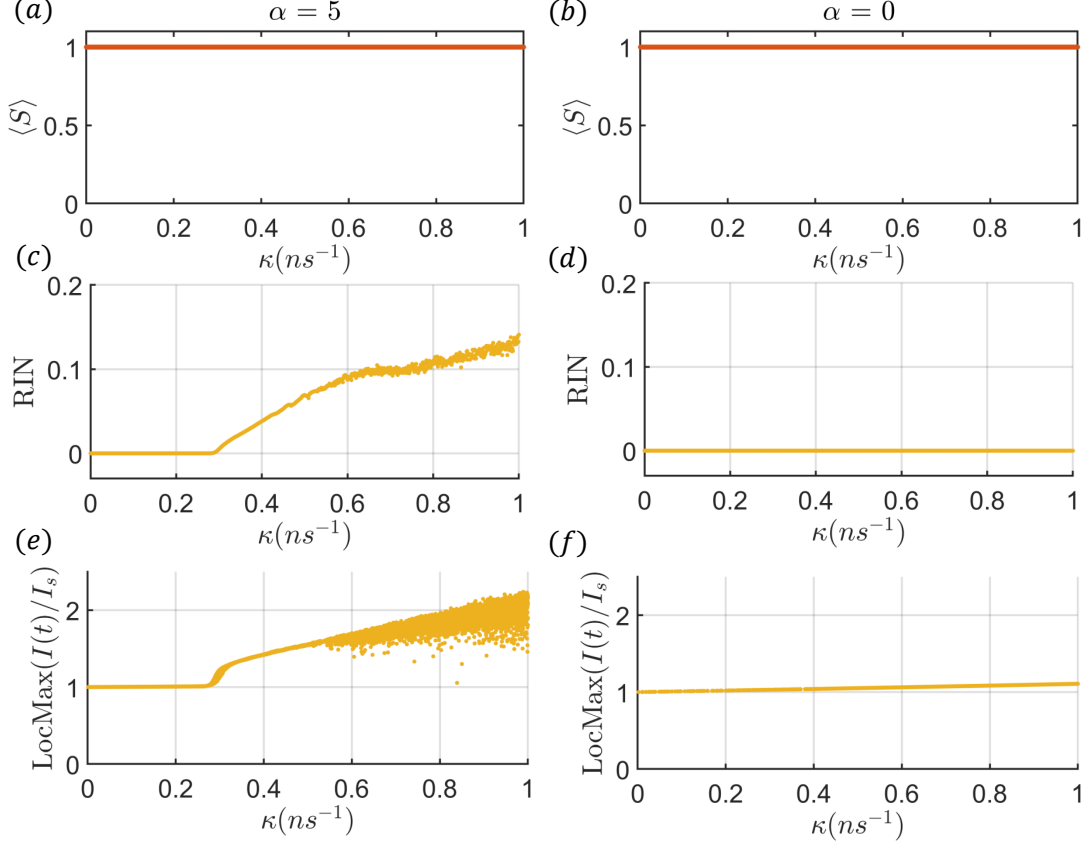


FIG. S1. Without frequency disorder, homogeneous all-to-all coupling yields complete synchronization, while nonzero amplitude–phase coupling  $\alpha$  drives chaotic synchronization as the coupling increases. Panels (a,c,e) and (b,d,f) show, for  $M = 24$ , the synchronization measure  $\langle S \rangle$ , the relative intensity noise (RIN), i.e., the variance of normalized intensity fluctuations  $(I(t) - \langle I \rangle)/\langle I \rangle$ , and the local maximum of the normalized intensity for each laser  $i$ , as functions of  $\kappa$  for  $\alpha = 5$  and  $\alpha = 0$ . The time window is  $[50, 100]$  ns.

In the absence of frequency disorder ( $\Delta_i = \Delta_j = 0$ ) with all lasers oscillating at the reference frequency  $\omega_0$ , homogeneous all-to-all coupling  $K_{ij} = \kappa(1 - \delta_{ij})$  yields complete synchronization with  $\langle S \rangle = 1$  for arbitrary  $\kappa$ . The underlying dynamics, however, depend on the amplitude–phase coupling  $\alpha$ . For  $\alpha = 0$ , the system reduces approximately to pure phase dynamics governed by the Kuramoto model, leading to steady-state synchronization independent of  $\kappa$ . By contrast, nonzero  $\alpha$  in the Lang–Kobayashi (LK) equations drives the system into chaotic synchronization once the coupling enters the strong regime ( $\kappa \gtrsim 1 \text{ ns}^{-1}$ ) [25, 33].

## Appendix B: Disorder-induced resonance and chaos driven by amplitude–phase coupling

In the main text, we develop the thermodynamic potential theory to analyze the structure of near-synchronized steady states. Based on the critical coupling strength, this framework explains both the scaling behavior of synchronization resonance at the optimal coupling value  $\kappa^*$  and the independence of the synchronized peak  $\langle S \rangle_{\text{max}}$  from the number of lasers  $M$ . However, the specific optimal coupling  $\kappa^*$ —typically larger than the critical value  $\kappa_c$ —is determined by the onset of chaotic dynamics beyond the steady state. This chaotic behavior, induced by the amplitude–phase coupling factor  $\alpha$  (see Fig. S2), is the direct reason synchronization resonance emerges under frequency disorder. Consequently, in the strong-coupling regime, although numerous near-synchronized steady states exist in both the LK equation and the Kuramoto model, these states are unstable chaotic attractors in the LK system due to nontrivial amplitude–phase coupling, but remain stable fixed points in the pure phase dynamics of the Kuramoto model.



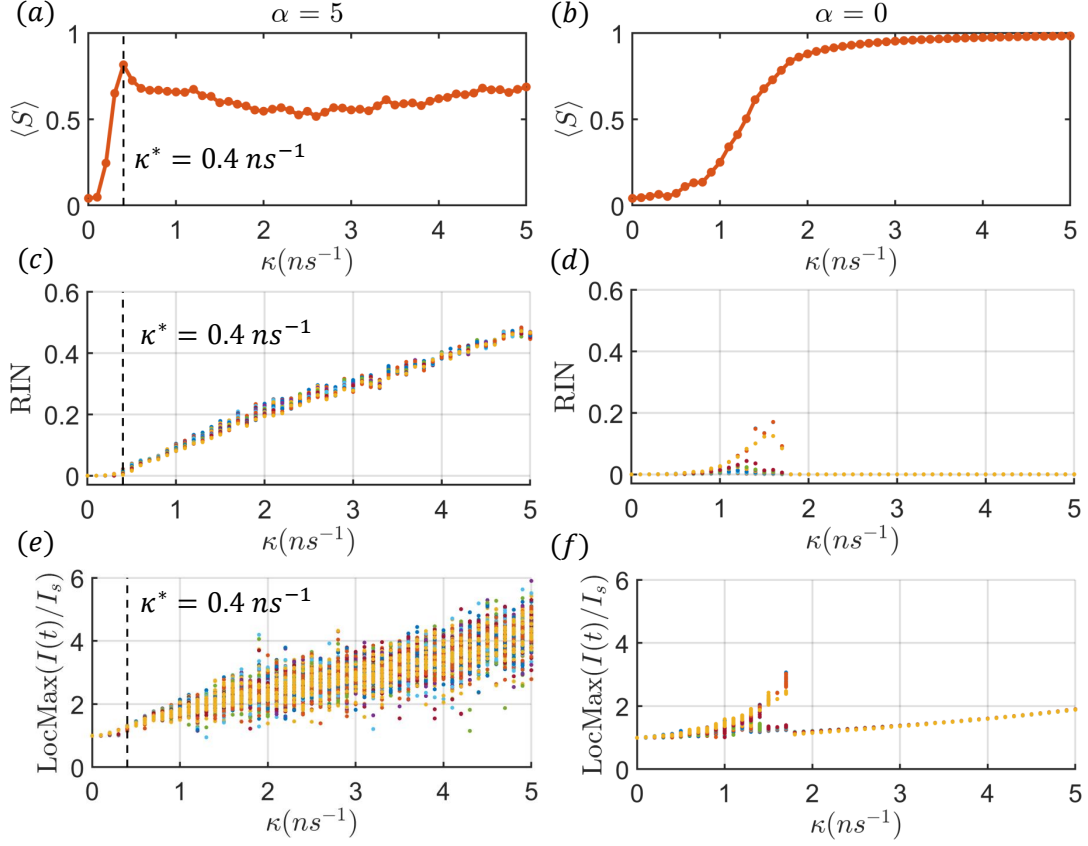


FIG. S2. Under frequency disorder, the amplitude–phase coupling induces chaotic dynamics in the strong-coupling regime, leading to the emergence of synchronization resonance in the LK equation—an effect absent in the purely phase-based dynamics of the classical Kuramoto model. Panels (a,c,e) and (b,d,f) show, for  $M = 24$ , the synchronization measure  $\langle S \rangle$ , the relative intensity noise (RIN), i.e., the variance of normalized intensity fluctuations  $(I(t) - \langle I \rangle)/\langle I \rangle$ , and the local maximum of the normalized intensity for each laser  $i$ , as functions of  $\kappa$  for  $\alpha = 5$  and  $\alpha = 0$ . The time horizon is  $[150, 200]$  ns.

### Appendix C: Effective thermodynamic potential for the laser network

Starting from the coupled LK equation in Eq. (1), we express the electric field in the polar coordinates as  $E_i(t) = r_i(t)e^{i\Omega_i(t)}$ , where  $r_i(t)$  and  $\Omega_i(t)$  are the amplitude and phase, respectively. To separate the radial and angular components, we multiply both sides of the complex electric field equation by  $e^{-i\Omega_i(t)}/r_i(t)$ . The real and imaginary parts of the resulting expression correspond to the amplitude and phase dynamics, respectively. The resulting coupled LK equations in the polar coordinates [19] is

$$\begin{aligned}
 \frac{\dot{r}_i(t)}{r_i(t)} &= \frac{1}{2}[G(N_i(t), r_i(t)) - \gamma] + \sum_{j=1}^M K_{ij} \frac{r_j(t-\tau)}{r_i(t)} \cos[\Omega_j(t-\tau) - \Omega_i(t) - \omega_0\tau], \\
 \dot{\Omega}_i(t) &= \frac{\alpha}{2}[G(N_i(t), r_i(t)) - \gamma] + \Delta_i + \sum_{j=1}^M K_{ij} \frac{r_j(t-\tau)}{r_i(t)} \sin[\Omega_j(t-\tau) - \Omega_i(t) - \omega_0\tau], \\
 \frac{\dot{N}_i(t)}{N_i(t)} &= \frac{J_0}{N_i(t)} - \gamma_n - \frac{G(N_i(t), r_i(t))r_i^2(t)}{N_i(t)},
 \end{aligned} \tag{S1}$$

where the gain function is defined as

$$G(N_i(t), r_i(t)) = g \frac{N_i(t) - N_0}{1 + s r_i^2(t)}.$$

Since we are only concerned with the steady state, we now expand the solutions around it:

$$r_i(t) \approx r_i^s, \quad N_i(t) \approx N_i^s, \quad \text{and} \quad \frac{r_j(t-\tau)}{r_i(t)} \approx 1. \quad (\text{S2})$$

Under these approximations, the LK equations reduce to:

$$0 = \frac{1}{2}[G(N_i^s, r_i^s) - \gamma] + \sum_{j=1}^M K_{ij} \cos[\Omega_j(t-\tau) - \Omega_i(t) - \omega_0\tau], \quad (\text{S3})$$

$$\dot{\Omega}_i(t) = \frac{\alpha}{2}[G(N_i^s, r_i^s) - \gamma] + \Delta_i + \sum_{j=1}^M K_{ij} \sin[\Omega_j(t-\tau) - \Omega_i(t) - \omega_0\tau], \quad (\text{S4})$$

$$0 = \frac{J_0}{N_i^s} - \gamma_n - \frac{G(N_i^s, r_i^s)(r_i^s)^2}{N_i^s}. \quad (\text{S5})$$

Substituting the gain function from Eq. (S3) into Eq. (S4) eliminates the gain term in Eq. (S4), resulting in a phase equation that no longer explicitly depends on the gain. Consequently, the phase dynamics depend solely on the angular variables, effectively decoupling from both the amplitude and the carrier number. The resulting equation takes the form of the generalized time-delayed Kuramoto model [32] with an additional phase shift  $\tan^{-1} \alpha + \omega_0\tau$  and a dressed coupling enhanced by the amplitude-phase coupling  $\alpha$ :

$$\dot{\Omega}_i(t) = \Delta_i - \sqrt{1 + \alpha^2} \sum_{j=1}^M K_{ij} \sin[\Omega_i(t) - \Omega_j(t-\tau) + \tan^{-1} \alpha + \omega_0\tau]. \quad (\text{S6})$$

To derive the effective thermodynamic potential, we transform Eq. (S6) into the following gradient flow form:

$$\dot{\eta}_i(t) = -\frac{1}{\tau} \frac{d}{d\eta_i} U(\eta_i),$$

where the collective coupling influence of the other lasers on laser  $i$  is contained in the thermodynamic potential  $U(\eta_i)$ . The time-delayed phase difference can be defined as

$$\eta_{ij}(t) = \Omega_i(t) - \Omega_j(t-\tau).$$

Associated with the steady-state synchronization solution, the phase variables  $\Omega_i(t)$  and  $\Omega_j(t)$  are proximal to each other. The second-order tensor  $\eta_{ij}(t)$  of the phase differences can then be approximated by a vector  $\eta_i(t)$ :

$$\eta_i(t) \approx \Omega_i(t) - \Omega_i(t-\tau). \quad (\text{S7})$$

To proceed, we further assume a slow temporal evolution of the phase, so the finite difference can be approximated by the average derivative:

$$\frac{\eta_i(t)}{\tau} \approx \frac{\dot{\Omega}_i(t) + \dot{\Omega}_i(t-\tau)}{2}. \quad (\text{S8})$$

Combining Eqs. (S7) and (S8), we get

$$\eta_i(t) \approx \tau \dot{\Omega}_i(t) - \frac{1}{2} \tau \dot{\eta}_i(t). \quad (\text{S9})$$

Substituting this relation into the generalized time-delayed Kuramoto model [Eq. (S6)], we obtain:

$$\dot{\eta}_i(t) = -\frac{1}{\tau} \left[ 2\eta_i(t) - 2\tau\Delta_i + 2\tau\sqrt{1 + \alpha^2} \left( \sum_{j=1}^M K_{ij} \right) \sin[\eta_i(t) + \tan^{-1} \alpha + \omega_0\tau] \right]. \quad (\text{S10})$$

The effective thermodynamic potential can then be identified as:

$$U(\eta_i(t)) = \eta_i^2(t) - 2\tau\Delta_i\eta_i(t) - 2\tau\sqrt{1 + \alpha^2} k_i^{\text{in}} \cos[\eta_i(t) + \tan^{-1} \alpha + \omega_0\tau], \quad (\text{S11})$$



and  $k_i^{\text{in}} \equiv \sum_{j=1}^M K_{ij}$  denotes the intrinsic coupling strength coming from other lasers to the  $i$ -th laser. This expression generalizes the result for a single laser [27]:

$$U(\nu(t)) = \nu^2(t) - 2\tau\sqrt{1 + \alpha^2}\gamma \cos[\nu(t) + \tan^{-1}\alpha + \omega_0\tau], \quad (\text{S12})$$

where  $\gamma$  is the self-coupling strength and  $\nu(t) \equiv \Omega(t) - \Omega(t - \tau)$ . The thermodynamic potential in Eq. (S11) indicates that the effective coupling strength  $\mathbb{K}_i \equiv \tau\sqrt{1 + \alpha^2}k_i^{\text{in}}$  is governed by the time delay  $\tau$ , the amplitude-phase coupling factor  $\alpha$ , and the intrinsic coupling strength  $k_i^{\text{in}}$  (or  $\gamma$  for a single laser).

The local minima of the potential  $U(\eta_i(t))$  can be determined through the first and second derivatives with respect to  $\eta_i(t)$ :

$$\frac{dU(\eta_i(t))}{d\eta_i(t)} = \eta_i(t) - \tau\Delta_i + \mathbb{K}_i \sin[\eta_i(t) + \tan^{-1}\alpha + \omega_0\tau] = 0, \quad (\text{S13})$$

$$\frac{d^2U(\eta_i(t))}{d\eta_i^2(t)} = 1 + \mathbb{K}_i \cos[\eta_i(t) + \tan^{-1}\alpha + \omega_0\tau] > 0. \quad (\text{S14})$$

Setting  $\omega_0\tau \equiv 2N\pi$ , Eqs. (S13) and (S14) can be further simplified as

$$\eta_i - \mathbb{F}_i = -\mathbb{K}_i \sin(\eta_i + \phi), \quad (\text{S15})$$

$$1 + \mathbb{K}_i \cos(\eta_i + \phi) > 0, \quad (\text{S16})$$

where  $\mathbb{F}_i \equiv \tau\Delta_i$  denotes the effective detuning, and the constant phase shift due to nonzero amplitude-phase coupling, is defined as

$$\phi \equiv \text{mod}(\tan^{-1}\alpha + \omega_0\tau, 2\pi) \approx 0.4\pi.$$

The cross intersections from Eq. (S15) correspond to the phase difference

$$\eta_i^*(t) \approx \Omega_i^{fit}\tau + \varphi_i(t) - \varphi_i(t - \tau)$$

for each laser  $i$ . In the case of complete frequency and phase synchronization among lasers, the solutions are expected to be independent of laser index  $i$  and this simplifies to

$$\eta^* \approx \Omega^{fit}\tau = 2\pi f_{\text{final}}\tau,$$

under the approximation  $\varphi(t) \approx \varphi(t - \tau)$ , which renders  $\eta$  time-independent. To compensate for frequency disorders and ensure that  $\eta^*$  is independent of the laser index  $i$ , the effective coupling must be sufficiently strong: For an arbitrary laser  $i$ , the effective coupling strength should exceed the effective detuning, i.e.,  $\mathbb{K}_i > |\mathbb{F}_i|$ , or equivalently

$$k_i^{\text{in}} > |\Delta_i|/\sqrt{1 + \alpha^2}$$

so that all solutions  $\eta_i$  fall within a similar and narrow range satisfying  $1 + \mathbb{K}_i \cos(\eta_i + \phi) > 0$ , and remain close to the initial mean frequency across general network configurations.

The variational principle stipulates that the system's dynamics relax toward the global minimum or, when separated by appreciable barriers, to local minima of the potential. With or without  $\alpha$ , the steady-state solution structure remains qualitatively similar, but is shifted by the additional phase and modified by the dressed coupling due to amplitude-phase coupling  $\alpha$ . However, the LK equations determine the dynamical stability: nonzero amplitude-phase coupling  $\alpha$  destabilizes the steady states and drives them into chaotic attractors, whereas in its absence the steady states remain stable, as shown in previous sections.

- 
- [1] Y. Kuramoto, *Chemical Oscillations, Waves, and Turbulence* (Springer, Berlin, 1984).
  - [2] A. Pikovsky, M. Rosenblum, and J. Kurths, *Synchronization: A Universal Concept in Nonlinear Science* (Cambridge University Press, Cambridge, 2003).
  - [3] L. M. Pecora and T. L. Carroll, Master stability functions for synchronized coupled systems, *Phys. Rev. Lett.* **80**, 2109 (1998).
  - [4] L. Huang, Q. Chen, Y.-C. Lai, and L. M. Pecora, Generic behavior of master-stability functions in coupled nonlinear dynamical systems, *Phys. Rev. E* **80**, 036204 (2009).

- [5] S. Watanabe and S. H. Strogatz, Integrability of a globally coupled oscillator array, *Phys. Rev. Lett.* **70**, 2391 (1993).
- [6] E. Ott and T. M. Antonsen, Low dimensional behavior of large systems of globally coupled oscillators, *Chaos* **18**, 037113 (2008).
- [7] C. R. S. Williams, T. E. Murphy, R. Roy, F. Sorrentino, T. Dahms, and E. Schöll, Experimental observations of group synchrony in a system of chaotic optoelectronic oscillators, *Phys. Rev. Lett.* **110**, 064104 (2013).
- [8] C. Williams, F. Sorrentino, T. E. Murphy, and R. Roy, Synchronization states and multistability in a ring of periodic oscillators: Experimentally variable coupling delays, *Chaos* **23**, 143117 (2013).
- [9] J. D. Hart, J. P. Pade, T. Pereira, T. E. Murphy, and R. Roy, Adding connections can hinder network synchronization of time-delayed oscillators, *Phys. Rev. E* **92**, 022804 (2015).
- [10] Y. C. Ji, I. Uzelac, N. Otani, S. Luther, R. F. J. Gilmour, E. Cherry, and F. Fenton, Synchronization as a mechanism for low-energy anti-fibrillation pacing, *Heart Rhyt.* **14**, 1254 (2017).
- [11] Parallel to the development of modern network science that started about 25 years ago, synchronization in complex networks has been extensively studied [37], due to the rich variety of complex network structures in natural and engineering systems and the fundamental role of synchronous dynamics in the system functioning. Earlier it was found that small-world networks, due to their small network diameter values, are more synchronizable than regular networks of comparable sizes [38], but heterogeneity in the network structure presents an obstacle to synchronization [39]. Subsequently it was found that heterogeneous networks with weighted links can be more synchronizable than small-world and random networks [40]. The onset of chaotic phase synchronization in complex networks of coupled heterogeneous oscillators was also studied [41]. The interplay between network symmetry and synchronization was uncovered and understood [42–44]. In complex networks, the transition from desynchronization to synchronization is typically continuous, e.g., the synchronization error or the order parameter tends to change continuously through the critical point, which is characteristic of a second-order phase transition. However, studies of networked systems of coupled phase oscillators revealed that, if the network links are weighted according to the natural frequencies of the oscillators, the transition can be abrupt and discontinuous, i.e., a first-order phase transition [45–48]. This phenomenon, known as explosive synchronization, is proof of the strong influence of network structure on the collective dynamics. It has also been established mathematically that random temporal coupling can promote network synchronization [49].
- [12] S. F. Brandt, B. K. Dellen, and R. Wessel, Synchronization from disordered driving forces in arrays of coupled oscillators, *Phys. Rev. Lett.* **96**, 034104 (2006).
- [13] Y. Zhang and A. E. Motter, Identical synchronization of nonidentical oscillators: when only birds of different feathers flock together, *Nonlinearity* **31**, R1 (2018).
- [14] Y. Zhang, J. L. Ocampo-Espindola, I. Z. Kiss, and A. E. Motter, Random heterogeneity outperforms design in network synchronization, *Proc. Natl. Acad. Sci. (USA)* **118**, e2024299118 (2021).
- [15] Y. Zhang, Y. Sugitani, and A. E. Motter, Synchronizing chaos with imperfections, *Phys. Rev. Lett.* **126**, 164101 (2021).
- [16] A. Nazerian, S. Panahi, and F. Sorrentino, Synchronization in networked systems with large parameter heterogeneity, *Commun. Phys.* **6**, 253 (2023).
- [17] A. Argyris, M. Bourmpos, and D. Syvridis, Experimental synchrony of semiconductor lasers in coupled networks, *Opt. Express* **24**, 5600 (2016).
- [18] B. Kim, N. Li, A. Locquet, and D. Citrin, Experimental bifurcation-cascade diagram of an external-cavity semiconductor laser, *Opt. Express* **22**, 2348 (2014).
- [19] N. Nair, K. Hu, M. Berrill, K. Wiesenfeld, and Y. Braiman, Using disorder to overcome disorder: A mechanism for frequency and phase synchronization of diode laser arrays, *Phys. Rev. Lett.* **127**, 173901 (2021).
- [20] O. Spitz, S. Koyu, P. Nyaupane, M. Berrill, and Y. Braiman, Complex spatio-temporal non-linear dynamics in a 1d-array of 23 broad-area semiconductor laser diodes under external optical feedback, in *Laser Technology for Defense and Security XVIII*, Vol. 12515 (SPIE, 2023) pp. 14–21.
- [21] S. Koyu, O. Spitz, M. A. Berrill, and Y. Braiman, Dynamics and phase-locking in large heterogeneous arrays of semiconductor diode lasers, in *High-Power Diode Laser Technology XXI*, Vol. 12403 (SPIE, 2023) pp. 199–215.
- [22] L. Zhang, W. Pan, L. Yan, B. Luo, X. Zou, and S. Li, Isochronous synchronization induced by topological heterogeneity in semiconductor laser networks, *Opt. Laser Technol.* **153**, 108243 (2022).
- [23] J. Tian-alsina and C. Masoller, Dynamics of a semiconductor laser with feedback and modulation: Experiments and model comparison, *Opt. Express* **30**, 9441 (2022).
- [24] T. Niiyama and S. Sunada, Power-law fluctuations near critical point in semiconductor lasers with delayed feedback, *Phys. Rev. Res.* **4**, 043205 (2022).
- [25] H. G. Winful and L. Rahman, Synchronized chaos and spatiotemporal chaos in arrays of coupled lasers, *Phys. Rev. Lett.* **65**, 1575 (1990).
- [26] P. Alsing, V. Kovanis, A. Gavrielides, and T. Erneux, Lang and Kobayashi phase equation, *Phys. Rev. A* **53**, 4429 (1996).
- [27] D. Lenstra, Statistical theory of the multistable external-feedback laser, *Opt. Commun.* **81**, 209 (1991).
- [28] R. L. Davidchack, Y.-C. Lai, A. Gavrielides, and V. Kovanis, Chaotic transitions and low-frequency fluctuations in semiconductor lasers with optical feedback, *Physica D: Nonlinear Phenom.* **145**, 130 (2000).
- [29] R. Lang and K. Kobayashi, External optical feedback effects on semiconductor injection laser properties, *IEEE J. Quantum Electron.* **16**, 347 (1980).
- [30] N. Nair, E. Bochove, and Y. Braiman, Almost perfect in-phase and anti-phase chaotic and periodic phase synchronization in large arrays of diode lasers, *Opt. Commun.* **430**, 104 (2019).
- [31] N. Nair, E. Bochove, and Y. Braiman, Phase-locking of arrays of weakly coupled semiconductor lasers, *Opt. Exp.* **26**, 20040 (2018).

- [32] M. S. Yeung and S. H. Strogatz, Time delay in the kuramoto model of coupled oscillators, *Phys. Rev. Lett.* **82**, 648 (1999).
- [33] H. G. Winful and S. S. Wang, Stability of phase locking in coupled semiconductor laser arrays, *Appl. Phys. Lett.* **53**, 1894 (1988).
- [34] N. Chopra and M. W. Spong, On exponential synchronization of Kuramoto oscillators, *IEEE Trans. Autom. Control* **54**, 353 (2009).
- [35] A. Jadbabaie, N. Motee, and M. Barahona, On the stability of the Kuramoto model of coupled nonlinear oscillators, in *Proc. Amer. Control Conf. (ACC), 2004*, Vol. 5 (IEEE, 2004) pp. 4296–4301.
- [36] F. Dörfler and F. Bullo, On the critical coupling for kuramoto oscillators, *SIAM J. Appl. Dyn. Syst.* **10**, 1070 (2011).
- [37] A. Arenas, A. Díaz-Guilera, J. Kurths, Y. Moreno, and C. S. Zhou, Synchronization in complex networks, *Phy. Rep.* **469**, 93 (2008).
- [38] M. Barahona and L. M. Pecora, Synchronization in small-world systems, *Phys. Rev. Lett.* **89**, 054101 (2002).
- [39] T. Nishikawa, A. E. Motter, Y.-C. Lai, and F. C. Hoppensteadt, Heterogeneity in oscillator networks: Are smaller worlds easier to synchronize?, *Phys. Rev. Lett.* **91**, 014101 (2003).
- [40] X. G. Wang, Y.-C. Lai, and C. H. Lai, Enhancing synchronization based on complex gradient networks, *Phys. Rev. E* **75**, 056205 (2007).
- [41] F. Ricci, R. Tonelli, L. Huang, and Y.-C. Lai, Onset of chaotic phase synchronization in complex networks of coupled heterogeneous oscillators, *Phys. Rev. E* **86**, 027201 (2012).
- [42] L. M. Pecora, F. Sorrentino, A. M. Hagerstrom, T. E. Murphy, and R. Roy, Cluster synchronization and isolated desynchronization in complex networks with symmetries, *Nat. Commun.* **5**, 4079 (2014).
- [43] F. Sorrentino, L. M. Pecora, A. M. Hagerstrom, T. E. Murphy, and R. Roy, Cluster synchronization and isolated desynchronization in complex networks with symmetries, *Sci. Adv.* **2**, e1501737 (2016).
- [44] J. D. Hart, Y. Zhang, R. Roy, and A. E. Motter, Topological control of synchronization patterns: Trading symmetry for stability, *Phys. Rev. Lett.* **122**, 058301 (2019).
- [45] J. Gómez-Gardeñes, S. Gómez, A. Arenas, and Y. Moreno, Explosive synchronization transitions in scale-free networks, *Phys. Rev. Lett.* **106**, 128701 (2011).
- [46] Y. Zou, T. Pereira, M. Small, Z. Liu, and J. Kurths, Basin of attraction determines hysteresis in explosive synchronization, *Phys. Rev. Lett.* **112**, 114102 (2014).
- [47] S. Boccaletti, J. A. Almendral, S. Guan, I. Leyva, Z. Liu, I. Sendiña-Nadal, Z. Wang, and Y. Zou, Explosive transitions in complex networks' structure and dynamics: Percolation and synchronization, *Phys. Rep.* **660**, 1 (2016).
- [48] Y.-S. Long, Z.-M. Zhai, M. Tang, and Y.-C. Lai, Metamorphoses and explosively remote synchronization in dynamical networks, *Chaos* **32**, 043110 (2022).
- [49] S. Zhou, Y. Guo, M. Liu, Y.-C. Lai, and W. Lin, Random temporal connections promote network synchronization, *Phys. Rev. E* **100**, 032302 (2019).